BBA - General Subjects 1863 (2019) 1513–1523

Contents lists available at ScienceDirect

BBA - General Subjects

journal homepage: www.elsevier.com/locate/bbagen

Influence of pulse characteristics and power density on stratum corneum permeabilization by dielectric barrier discharge

Monika Gelker[a,b,*], Julia Mrotzek[a,d], Astrid Ichter[a,d], Christel C. Müller-Goymann[b,c], Wolfgang Viöl[a]

[a] Department of Sciences and Technology, HAWK University of Applied Sciences and Arts, Von-Ossietzky-Str. 99, 37085 Göttingen, Germany
[b] PVZ – Center of Pharmaceutical Engineering, Technische Universität Braunschweig, Franz-Liszt-Str. 35a, 38106 Braunschweig, Germany
[c] Institut Pharmazeutische Technologie, Technische Universität Braunschweig, Mendelssohnstrasse 1, 38106 Braunschweig, Germany
[d] Fraunhofer IST, Application Center for Plasma and Photonics, Von-Ossietzky-Str. 100, 37085 Göttingen, Germany

ARTICLE INFO

Keywords:
Direct cold atmospheric plasma
Dielectric barrier discharge
Skin permeabilization
Drug transport
Transepithelial electrical resistance
Franz cell permeation

ABSTRACT

Background: In recent years, the medical use of cold atmospheric plasma has received much attention. Plasma sources can be suited for widely different indications depending on their physical and chemical characteristics. Being interested in the enhancement of drug transport across the skin by plasma treatment, we evaluated three dielectric barrier discharges (DBDs) as to their potential use in permeabilizing human isolated stratum corneum (SC).

Methods: Imaging techniques (electrochemical and redox-chemical imaging, fluorescence microscopy), transepithelial electrical resistance measurements and permeation studies were employed to study the permeabilizing effect of different DBD-treatments on SC.

Results: Filamentous µs-pulsed DBDs induced robust pore formation in SC. Increasing the power of the µs-pulsed DBD lead to more pronounced pore formation but might increase the risk of undesired side-effects. Plasma permeabilization was much smaller for the ns-pulsed DBD, which left SC samples largely intact.

Conclusions: The comparison of different DBDs provided insight into the mechanism of DBD-induced SC permeabilization. It also illustrated the need to tailor electrical characteristics of a DBD to optimize it for a particular treatment modality. For future applications in drug delivery it would be beneficial to monitor the permeabilization during a plasma treatment.

General significance: Our results provide mechanistic insight into the potential of an emerging interdisciplinary technology – plasma medicine – as a prospective tool or treatment option. While it might become a safe and pain-free method to enhance skin permeation of drug substances, this is also a mechanism to keep in mind when tailoring plasma sources for other uses.

1. Introduction

Cold atmospheric plasma (CAP), among many possible biomedical applications, has been shown to permeabilize human skin. Therefore, current research aims at the development of CAP sources as a safe, pain-free and non-invasive method to enhance transcutaneous drug delivery.

In order to pass through the skin and reach the site of action, drug molecules must first and foremost pass the stratum corneum (SC). This topmost layer of the skin forms the main protective barrier towards the environment and its composition is popularly described by the 'brick and mortar' model: Several layers of proteinaceous remnants of cornified keratinocytes are surrounded by and connected to a lipid matrix. Thus, a method of permeabilization needs to create pores spanning all layers of the SC. Several methods to facilitate transdermal drug delivery are already well known. Some, like iontophoresis or occlusion patches, work mainly for relatively small molecules towards which the SC is already more or less permeable. But several physical methods have been shown to achieve pore formation through SC. Among these are microneedling [1], electroporation [2], sonoporation [3] or plasmaporation – permeabilization of the skin using CAP.

CAP is basically a weakly ionized gas (here the gas is ambient air), which is formed when energy, e.g. in the form of a high electric field, accelerates free electrons to cause partial ionization of molecules and atoms. This increases the density of free electrons, which are further

* Corresponding author at: HAWK University of Applied Sciences and Arts, Department of Sciences and Technology, Von-Ossietzky-Str. 99, 37085 Göttingen, Germany.
E-mail address: monika.gelker@hawk.de (M. Gelker).

https://doi.org/10.1016/j.bbagen.2019.05.014
Received 8 March 2019; Received in revised form 13 May 2019; Accepted 21 May 2019
Available online 23 May 2019

accelerated, causing an avalanche of ionization. The inclusion of a dielectric barrier in front of at least one electrode in the plasma source leads to the attenuation of the electric field as a result of the current flow causing charge accumulation on the dielectric, which quickly ends the discharge. This prevents an excessive increase in gas temperature and keeps the plasma 'cold'. In order to maintain the discharge, an alternating voltage signal is used, leading to the repeated formation of transient discharges. Accelerated electrons and ions facilitate a multitude of chemical reactions. In ambient air these charged species, together with reactive oxygen and nitrogen species (RONS), the electrical field and current as well as low intensity UV radiation, form a 'cocktail' of possible mechanisms to interact with biological tissues. These mechanisms may work together for enhanced permeabilization effectiveness [4,5]. Additional beneficial effects have been reported for a CAP treatment of the skin in the treatment of various diseases [6], such as an increase in microcirculation [7,8], skin acidification [9], the possible alleviation of pain or itch [10], or even an increase in skin wettability [11]. These may be used synergistically in future treatment modalities.

Research efforts have concentrated on the application of various CAP sources for skin permeabilization, among which are plasma jets [12,13], microplasma arrays [14] and direct dielectric barrier discharge (DBD) setups [15,16]. The latter being our configuration of choice for this study. We aimed to elucidate which plasma parameters influence permeabilization efficiency qualitatively and quantitatively. In our first study [5] we established that pore formation by dielectric barrier discharge (DBD) is possible and according to our hypothesis this is caused by local phase transition of SC lipids in the local high intensity filamentous regions of the discharge due to Joule heating. This is further investigated in the work reported here. In addition to various imaging techniques and measurements of permeability highlighting the distribution and dimensions of pores in isolated human SC, we also compared three DBDs (one ns-pulsed and two µs-pulsed DBDs) and characterized them electrically, physically and chemically to gain further insight into the underlying mechanism of plasma permeabilization.

2. Materials and methods

2.1. Skin samples and stratum corneum preparation

Human skin samples were obtained from patients undergoing abdominal plastic surgery (Department of Trauma-, Orthopedic- and Plastic Surgery, University Medical Center Göttingen, Germany). All donors gave their oral and written informed consent prior to the procedure, and the experiments were performed according to the Declaration of Helsinki principles following ethics committee approval. The preparation of isolated stratum corneum (SC) were performed as in Gelker et al. [5] according to Kligman and Christophers [17].

For the experiments circular samples of 13–20 mm were punched out of the dried SC using a hollow punch and subsequently rehydrated in water.

2.2. Plasma sources

Three different plasma sources in the direct dielectric barrier discharge (di-DBD) mode, all operated in ambient air, were tested. In all arrangements a cylindrical copper electrode with a diameter of 8 mm covered by a 1 mm thick ceramic cylinder of Al_2O_3 was used. The spacing between the electrode and the grounded SC samples was kept at a distance of 1 mm (Fig. 1A). For two µs-pulsed DBDs a pulsed high-voltage power supply with a frequency of 300 Hz and adjustable amplitude was used. The first half wave of each pulse is characterized by a FWHM (full width at half maximum) of 1 µs, the following half-waves have a FWHM of 4 µs. This source was operated at peak voltages of 9.0 kV (LP µs-DBD) and of 11.3 kV (HP µs-DBD). The electrical power in the discharge was determined to be 264 ± 44 mW·cm^{-2} or 465 ± 32 mW·cm^{-2} respectively. For the ns-DBD a power supply with a frequency of 300 Hz and 28 ns FWHM was utilized. The peak voltage of 8.9 kV was comparable to that of the LP µs-DBD. The electrical power of 241 ± 22 mW·cm^{-2} was comparable to that of the LP µs-DBD.

2.3. Plasma characterization

2.3.1. Electrical and optical characterization

For the estimation of the energy dissipated into the discharge a current monitor 2877 (Pearson Electronics, Inc., Palo Alto, USA) and a high-voltage probe P6015A (Tektronix Inc., Beaverton, USA) connected to a DLM 2054 oscilloscope (Yokogawa Deutschland GmbH, Herrsching, Germany) were used. According to the *U·I*-method, the pulse energy was derived by integration of the product of total voltage $u_{(t)}$ and total current $i_{(t)}$ over the pulse duration T_{pulse}. The power density P_A was calculated by multiplication of frequency f and pulse energy divided by the active area A [18].

$$P_A = \frac{f}{A} \bullet \int_0^{T_{pulse}} u_{(t)} \bullet i_{(t)}\, dt$$

Given values are mean values with standard deviation. Characteristic pulses (averaged over 128 single pulses) of the three DBDs are shown in Fig. 1B, next to representative photographs of the discharges (Fig. 1C). The discharge images were taken with a Nikon D90 camera with f/6.7 aperture, ISO sensitivity 800, focal length 85 mm and 1 s exposure time.

2.3.2. Optical emission spectroscopy and temperature measurements

Optical emission spectroscopy was used to determine rotational, vibrational and electron temperatures. Plasma temperatures are important reference values in the comparison of plasma sources and provide an insight into the plasma chemical processes [19,20]. All spectra were taken using an Echelle spectrometer (Aryelle-Butterfly 400; LTB Lasertechnik Berlin GmbH, Berlin, Germany) with a resolution of < 80 pm, which was calibrated to wavelength and relative intensity [21,22]. The optical fiber used for measurements was aligned centered to the discharge. For each plasma source five spectra with an exposure time of 60 s were collected. For further analysis, spectra were dark corrected and summated.

Determination of the temperatures and error estimation was carried out as described before [22,23]: For the rotational temperature the rotational structure of the 0–0 vibrational transition of the second positive system (C3Πu-B3Πg) of nitrogen in the wavelength range of 334.0 nm to 336.9 nm was compared to simulated spectra. The Boltzmann plot method was applied to derive vibrational temperatures. Electron temperature as well as electrical field strength and mean electron energy were obtained as previously described [24–26]. Additionally, the gas temperature near the discharge gap was determined using a fiber optic temperature sensor, FOT-L-SD and a UMI4 Universal Multichannel Instrument (both FISO Technologies Inc., Quebec, Canada).

2.3.3. Ozone measurement

Ozone concentrations were measured by absorption spectroscopy using the Ozone Monitor 106-L (2B Technologies, Inc., Boulder, USA). This model measures the ozone concentration at the wavelength of maximum absorption in the Hartley Band at 254 nm and was run at a flow rate of approx. 1 L·min^{-1} [27,28]. The ozone concentration was measured at lateral distances of 1–15 cm to the discharge in intervals of 10 s over a time period of 90 s. For each run the values between 40 s and 90 s were averaged. In total 3–4 measurements were recorded for each plasma source and data reported as mean ± standard deviation of the averaged values.

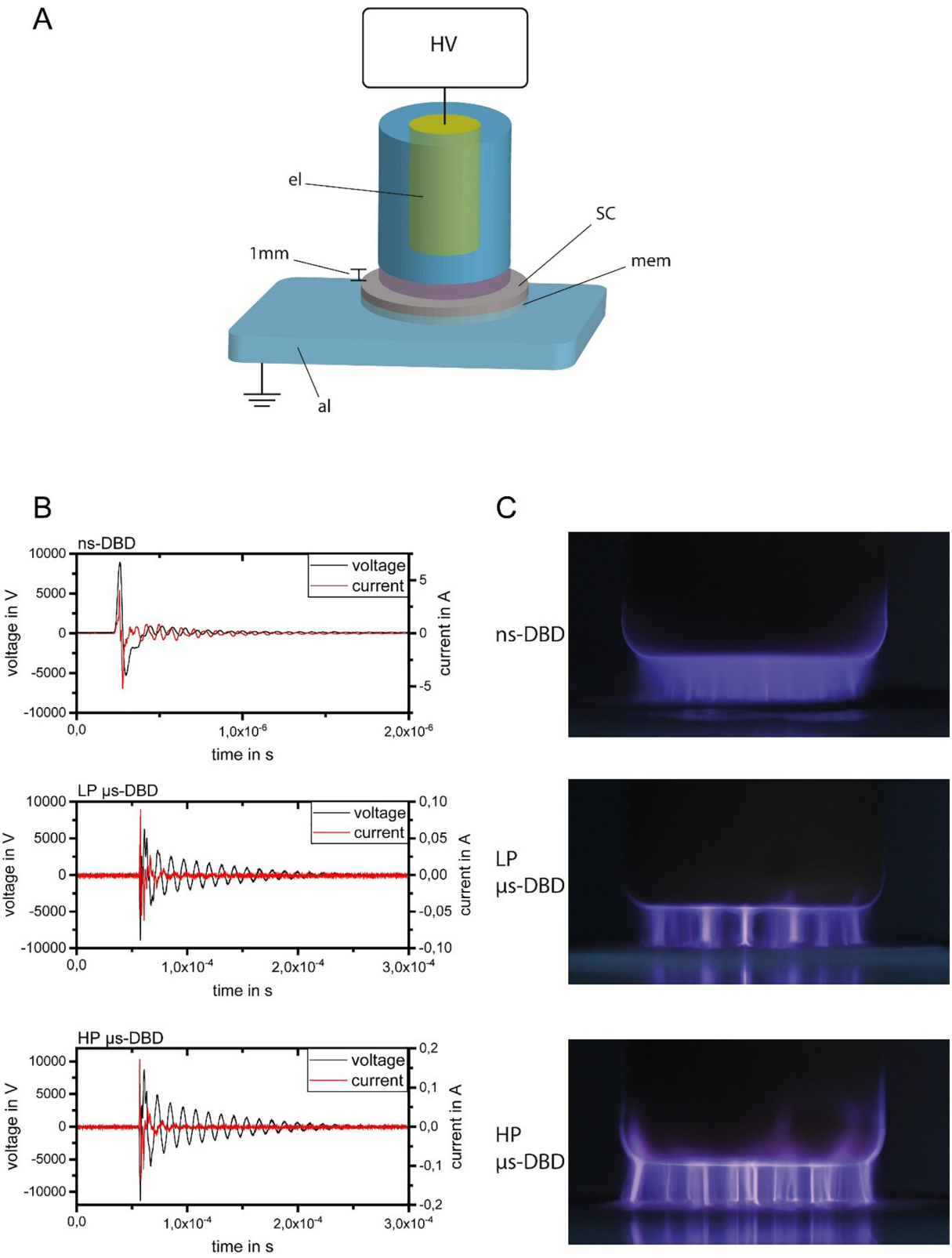

Fig. 1. Plasma treatment and plasma characterization. A) Direct DBD treatment of isolated human stratum corneum on iodide-starch paper or a porous membrane. HV) High voltage generator; SC) Stratum corneum; mem) porous membrane or iodide-starch paper; al) aluminum grounded electrode; 1 mm) gas gap of 1 mm; el) copper electrode enclosed by ceramic dielectric. B) Single exemplary pulses for all three DBDs used in this study (traces represent the mean of 128 pulses). C) Photographs of the three discharges. All images were taken with equal camera settings and 1 s exposure time.

2.4. Plasma treatment of isolated human stratum corneum

For the plasma treatment, SC samples were placed on a stabilizing membrane (porous polycarbonate) or on iodide-starch paper and acted as the second electrode in the setup. An aluminum grounded electrode underneath was necessary to maintain the discharge (see setup in Fig. 1A). One DBD-treatment usually consisted of two 90 s intervals of plasma with an intermittent pause of 10 min.

Using the ns-DBD and the LP µs-DBD an area of 0.5 cm^2 in the center of each sample is treated and for the HP µs-DBD the discharge spreads somewhat further, effectively treating an area of 0.78 cm^2 (compare discharge images in Fig. 1C). During exploratory experiments, SC samples were also treated within modified Franz-diffusion cells (see Section 2.6).

2.5. Imaging of permeabilization

2.5.1. Iodide-starch gel imaging

In order to detect the permeation of oxidizing plasma species during the DBD-treatment, hydrated potassium iodide starch paper (Sigma-Aldrich, Düren, Germany) was placed underneath the SC during plasma treatments (see Fig. 1A). The oxidizing chemical species permeate the SC only at permeabilized sites. There they penetrate into the iodide starch paper and oxidize iodide to elemental iodine. Through the formation of polyiodide (e.g. I_3^-) and its intercalation into the helical structure of starch, blue-violet dots form and show the sites of pore formation. Photographs of the resulting patterns were taken with a Nikon D90 camera (F/6.7, ISO 800, f 85 mm, exposure time 1/15 s).

2.5.2. Electrolytic imaging

A second method to visualize pore formation by the DBD-treatment harnesses an electrolytic reaction at the surface of a polished silver sheet. The method according to Pliquett et al. [29] has been extensively described elsewhere [5]. Briefly, the DBD-treated SC was placed between a PBS-agarose gel block and a polished silver sheet (Fig. 2). As soon as a low voltage is applied, the current flow at the sites of decreased electrical resistance leads to the electrolytic oxidation of silver, resulting in the formation of localized dark spots. Consecutively, the silver sheet was imaged on an Axio Imager Z.2 microscope with an Axiocam 105 color camera (Carl Zeiss AG, Oberkochen, Germany) and a 10× objective (Plan-Neofluar, NA 0.3) in the 'tiles' mode. 208 individual pictures were merged to capture the entire area of interest.

2.5.3. Fluorescence imaging of test substance permeation

As a third imaging method the permeation of various hydrophilic and fluorescent test substances (see Table 1) through DBD-treated SC into a thin film was tested. Sodium fluorescein (NaFluo) and the FITC-labeled dextrans were obtained from Merck KGaA (Darmstadt, Germany); the nano- and microparticles were Fluoresbrite® Fluorescent carboxylated polystyrene microspheres (Polyscience Inc., Warrington, USA).

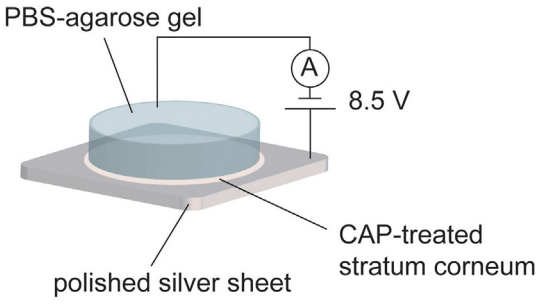

Fig. 2. Setup for electrolytic imaging of conductive regions after DBD-treatment.

As there was often a large degree of variation in the outcome of a DBD-treatment between skin donors as well as from sample to sample and from day to day, these experiments were carried out after iodide-starch imaging experiments (see Section 2.5.1) and a representative set of samples was subjected to the permeation. In some cases, the treatment deviated from the general protocol. While the treatment was usually 2 × 90 s as described in Section 2.4, in a few cases 1 × 180 s or 3 × 90 s were used as noted for the respective images (see Fig. 6).

The permeation setup consisted of a thin agarose gel film (0.5% low melting agarose in PBS) poured directly onto a microscope slide and forming the acceptor for the diffusion of test substances (0.5 mg·mL^{-1}, 500 µL), which were placed into specially designed glass donor compartments with an inner diameter of 10–12 mm. The DBD-treated (or untreated) SC samples with a diameter of 16–20 mm were sandwiched in between (Fig. 3B). To ensure that the fluorescence signal for the differently sized test substances was clearly visible without being oversaturated, it was necessary to use different incubation times (Table 1).

Images were taken with a Zeiss microscope Axio Observer Z1/7 with an EC Plan-Neofluar 10× / 0.3 Ph1 objective and the Axiocam 506 camera. Fluorescence was excited at 488 nm (filter 455–495 nm) and emission detected at 519 nm (filter 505–555 nm). In the 'tiles'-mode 160 images were combined to display the area of interest.

2.6. Measurement of transepithelial electrical resistance (TEER)

The transepithelial electrical resistance is a measure of the barrier function and therefore both an instrument of quality control and an indicator for the permeabilization caused by DBD-treatment. The method was implemented to be used with the modified Franz diffusion cells (Fig. 3A) according to the approach of Fokuhl and Müller-Goymann [30] and described in detail elsewhere [5]. Basically, custom-made Ag/AgCl double electrodes were connected to a voltohmmeter (EVOM2 with extended range, World Precision Instruments, Sarasota, USA), which produces an AC square wave current of ± 10 µA at 12.5 Hz, measures the resulting voltage and calculates the electrical resistance. The electrical resistance in Ω was normalized to the SC area. All values are reported in kΩ·cm^2. In large diffusion cells (15 mm inner diameter of the donor compartment) the TEER value could be determined before the DBD-treatment to check for intact barrier function and directly compared to the post-treatment TEER value. Since, in exploratory experiments, samples passing the visual inspection typically had very high TEER values as well and because the large samples needed for these experiments were often unstable over time and used up excessive amounts of donor skin, we utilized smaller Franz diffusion cells with an inner diameter of 8 mm and 13 mm SC samples for most experiments.

2.7. Franz diffusion cell permeation studies

In addition to the qualitative visualization of the permeation of variously sized test substances – ranging approx. from 1 nm to 2 µm (Table 1) – a quantitative approach using modified Franz diffusion cells [31] was followed (setup in Fig. 3A). The experimental protocol according to Täuber and Müller Goymann [32] as well as Lusiana et al. [33] has been described before [5] and was modified as follows:

Previous experiments had shown a nonlinear diffusion of test substances from PBS across µs-DBD-treated SC. In order to enable a more linear permeation and make use of a formulation more similar to something that would be used for pharmaceutical products, a hydrogel (Aquasonic 100 ultrasound transmission gel, Parker, USA) was employed as basis for the donor substance. This was mixed with PBS (1 part PBS on three parts hydrogel) and 500 µg·mL^{-1} fluorescent test substance (Table 1) to create a viscous but pipetteable fluid. The donor volume was 500 µL. From the acceptor compartment, samples of 250 µL (sets 1,2) or 100 µL (sets 3–5) were taken before the start of the

Table 1
Different fluorescent substances used for permeation imaging experiments with their properties, incubation time and exposure times during imaging.

Substance	Acronym	MW ($g \cdot mol^{-1}$)	Radius (nm)	Incubation time	Exposure time (ms)
Sodium fluorescein	NaFluo	332	–	< 1 min	9–10
FITC-dextran 4	FD4	4000	[a]1.4	10–15 min	550
FITC-dextran 40	FD40	40,000	[a]4.5	35–45 min	1000–1300
200 nm particles	200 nm	–	100	3–5 h	460
2 µm particles	2 µm	–	1000	6–10 h	30

[a] Stokes' radius according to supplier.

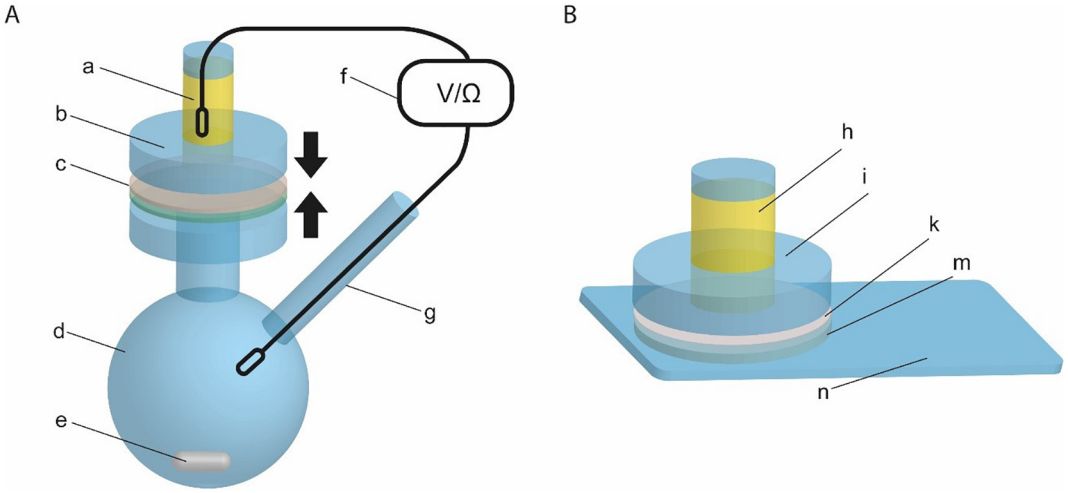

Fig. 3. Permeation of fluorescent test substances across DBD-treated SC. A) Modified Franz diffusion cell with electrodes for TEER measurements. a) test substance in hydrogel; b) donor compartment; c) isolated human stratum corneum; d) acceptor compartment; e) magnetic stirrer; f) voltohmmeter with two double electrodes for the determination of transepithelial electrical resistance values; g) sampling exit. B) Diffusion cell for imaging of localized transport of test substances across DBD-treated SC. h) test substance in hydrogel; i) donor compartment; k) isolated human stratum corneum; m) 0.5% PBS-agarose gel as acceptor on a microscope slide (n).

permeation and after 30 min, 2 h, 4 h, 6 h, 12 h and 24 h. Five sets of experiments were conducted and each set contained one experiment with each of the five test substances with skin from the same donor. All donors were female. They were aged 46 years (set 1), 47 years (set 2), 52 years (set 3) and 49 years (sets 4 and 5). Samples for each of the four treatment conditions (control, ns-DBD, LP µs-DBD, HP µs-DBD) were done in quadruplicate, resulting in $n = 20$ samples for each condition and every substance (see Section 2.10).

In addition to the hydrophilic permeations, an oil-based permeation was tested. In this case, the diffusion of the lipophilic fluorophore Nile Red (Sigma-Aldrich, Steinheim, Germany) through DBD-treated and untreated SC was investigated. The procedure, structure and apparatus were the same as in the previous permeation experiments with hydrophilic substances with exception of the medium for donor and acceptor, for which we used a paraffin-based oil (Penaten Pflegeöl, Neuss, Germany). The donor concentration of Nile Red was 0.1 $mg \cdot mL^{-1}$.

2.8. Measurement of nitrate and peroxides deposited on plasma-treated stratum corneum

When a plasma is ignited in ambient air, reactive oxygen and nitrogen species are produced. These can react with the treated surface or be adsorbed to the surface. The concentrations of two relatively stable species, peroxides and nitrate, were determined quantitatively with enzymatic test strips and a reflectometer (two-beam spectrometer RQflex 10 from Merck KGaA, Darmstadt, Germany) according to the manufacturer's instructions. Directly after the DBD-treatment, a 200 µL drop of water was added to the SC, solvating the adsorbed chemical compounds from the surface of the SC. For the peroxide measurements test strips with a range of 0.2–20.0 $mg \cdot L^{-1}$ were used, for the nitrate measurement the range was 3–90 $mg \cdot L^{-1}$. Due to the more unstable nature of peroxides as compared to nitrate, the peroxide concentration was always determined first.

2.9. Thermal images

Infrared imaging using a Variocam infrared camera (Infratec, Dresden, Germany) with Variocam II standard optics assessed the global heating of SC samples during plasma-treatment. Images were taken from above the sample within 2 s after a 90 s DBD treatment. Image analysis was performed using the software IRBIS 3 professional.

2.10. Statistical analysis

In general, experiments were repeated at least three times with at least three independent samples for each condition per experiment. Since the sample to sample variation was observed to be greater than the day to day variation, median and box plot data or arithmetic mean and standard deviation were calculated with every sample treated as an independent experiment. As a result of this, a given number n equals the total number of samples treated per condition in all experiments. As the data for peroxide and nitrate concentrations was normally distributed according to the Shapiro-Wilk test at the 0.05 level, they were further analyzed by ANOVA with post-hoc tests using the Bonferroni correction of *p*-values (using Origin 2018G, Origin Lab Corporation, Northampton, USA). TEER data were not normally distributed but could by analyzed in the same way according to the central limit theorem as the sample is very large. Permeation data were not normally distributed and thus further analyzed using the non-parametric median comparison with post-hoc stepwise comparison of the different DBD-treatments and the control (in IBM SPSS Statistics Version 24, IBM Corporation, Armonk, USA).

2.11. Key resource table

Resource	Source	Identifier
Biological sample		
Human skin	Department of Trauma-, Orthopedic- and Plastic Surgery, University Medical Center Göttingen, Germany	N/A
Chemical		
Fluoresbrite YG Carboxylate nano- and microparticles size range Kits I and II	Polysciences	Cat No. 21636 and 21,637
Fluorescein isothiocyanate–-dextran average MW 4000	Sigma	CAS Number 60842–46-8; Cat No. 46944
Fluorescein isothiocyanate–-dextran average MW 40,-000	Sigma	CAS Number 60842–46-8, Cat No. FD40S
Nile Red	Sigma	CAS Number 7385-67-3, Cat No. 72485
Potassium iodide starch paper	Sigma-Aldrich	Cat No. 37215
Silver sheet	Various	
Sodium fluorescein	Fluka	CAS Number 518–47-8, Cat No. 28803
Software		
Matlab	MathWorks	RRID:SCR_001622
Origin 2018G	Origin Lab Corporation	RRID:SCR_014212
Specair	SpectralFit S.A.S.	http://www.specair-radiation.net/
SPSS Statistics Version 24	IBM	RRID:SCR_002865
ZEN	Carl Zeiss GmbH	RRID:SCR_013672

3. Results and discussion

In recent years, several research groups have addressed the possibility to enhance drug transport through the skin with the aid of cold atmospheric plasma. While most publications on this topic use plasma jets or microplasma discharges, both of which are created independent of the skin surface above the treated area, we and a few others [15,16] concentrate on dielectric barrier discharges, which use skin as the counter electrode of the discharge circuit. The advantage of this configuration is immediacy of the treatment: As the plasma is created on the skin, all plasma components (electric field, current, charged particles, reactive chemical species etc.) reach the site on which they are supposed to act with minimal delay. On the other hand, in this configuration the exact properties of the discharge may vary depending on the skin properties. To minimalize these variations in our experiments we standardized our choice of skin samples as much as possible: Abdominal skin from healthy female donors between the ages of 45–52 years was used for all samples.

3.1. Plasma characterization

In previous experiments [5], we had seen that a µs-pulsed DBD (the same as the LP µs-DBD in this report) is capable of producing pores in isolated human stratum corneum (SC) and full-thickness skin. Consecutively we investigated the effect in greater depth, and therefore performed our experiments with two additional DBDs. A detailed electrical and spectroscopic characterization was performed in order to connect permeabilization data to the properties of the DBDs (see Table 2 for a comparison of various plasma parameters). One of the additional plasma sources had the same pulse characteristics as the LP µs-DBD (for low power µs-pulsed DBD) already used in the previous studies, but for a greater voltage amplitude and hence greater power density (HP µs-DBD for high power µs-pulsed DBD). The second additional discharge was a ns-pulsed DBD (furthermore referred to as ns-DBD). As can be seen in Fig. 1C, these three discharges primarily differ in the degree of filamentation. While the ns-DBD appears to be relatively homogeneous, the µs-DBDs form distinct macroscopic filaments, which are relatively stable during one treatment interval of 90 s. The reason for this lies in a much shorter rise-time of the ns-pulsed voltage, which means that the breakthrough criteria for the formation of a discharge are reached throughout the electrode area at the same time and many microscopically small filaments are formed. For the µs-pulsed DBDs the voltage rise-time is relatively long which leads to the formation of intense macroscopical filaments at fewer, stochastically distributed sites, or, in case of imperfections or irregularities on the treated surface (e.g. small hairs), at certain favored sites. These differences also show in the calculated rotational temperature, which is assumed to equal the gas temperature within the discharge, and in the vibrational temperature, which is connected to chemical processes in the discharge. While the rotational and vibrational temperatures for both µs sources are similar, values for the ns source are lower. With higher power density the values for mean electron energy are increasing for the µs-DBDs. Comparing the LP µs-DBD with the ns-DBD there is a notable difference in the electron temperatures despite their very similar power densities. In contrast to the rotational and vibrational temperature, the electron temperature is higher for the ns-pulsed DBD than for the LP µs-DBD. Measurements of the ozone concentration correlate with mean electron energy/ electron temperature (Table 2).

Table 2
Electrical, spectroscopic and chemical plasma parameters of the different plasma sources.

Parameter	LP µs-DBD	HP µs-DBD	ns-DBD
Pulse duration	70 µs	70 µs	200 ns
FWHM (full width at half maximum)	1 µs/4 µs	1 µs/4 µs	28 ns
Peak voltage (in kV)	9.0	11.3	8.9
Peak current (in A)[a]	0.90 ± 0.04	1.10 ± 0.00	9.4 ± 0.6
Power density (in $mW \cdot cm^{-2}$)	264 ± 44	465 ± 32	241 ± 22
Rotational temperature (in K)	385 ± 50	390 ± 50	325 ± 50
Vibrational temperature (in K)	2880 ± 221	2843 ± 208	2527 ± 220
Electron temperature (in 10^3 K)	44.5 ± 0.7	48.0 ± 0.3	46.3 ± 0.3
Mean electron energy (in eV)	5.75 ± 0.09	6.21 ± 0.04	5.91 ± 0.03
Reduced electrical field strength (in Td)	221 ± 5	247 ± 2	234 ± 2
$c(O_3)_{max}$ (in ppm)[b]	22 ± 7	40 ± 13	25 ± 12

[a] From single pulse recordings.
[b] Measured 1 cm from the discharge.

3.2. Visualization of plasma permeabilization and stability of pore formation

During the DBD treatment, the permeabilization of isolated human stratum corneum (SC) was made visible by oxidation of iodide and the resulting dark blue complex formed in iodide starch paper. Dark blue puncta appeared where the reactive oxygen or nitrogen species (RONS) produced in the discharge were able to pass through permeabilized SC and oxidize iodide (Fig. 4). Distinct permeabilized sites were detected for SC treated with both the LP µs-DBD and HP µs-DBD. Notably, an immediate permeabilization could never be detected for ns-DBD treatments.

Thus, it becomes clear that the power delivered to the skin by the plasma or the maximum voltage of a pulse, which are very similar for the ns-DBD and the LP µs-DBD, are not the most critical parameters for pore formation. The maximum current, which is distinctly higher for the ns-DBD than for both µs-DBDs, does not seem to play a prominent

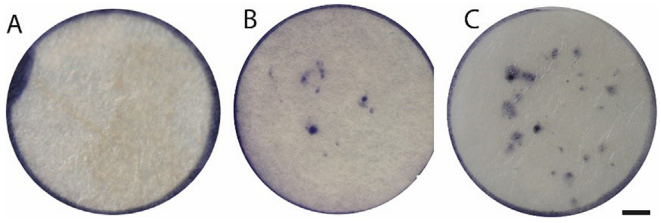

Fig. 4. Permeabilized regions in DBD-treated SC as visualized by transport of reactive chemical species through newly formed pores and oxidation of iodide with subsequent formation of a dark blue I_3^--starch complex. A) ns-pulsed DBD; B) LP µs-pulsed DBD; C) HP µs-pulsed DBD. The bar represents a length of 2 mm.

role either.

The persistence of the pores thus observed was visualized using an electrolytic approach. Through oxidation of a silver sheet below a SC sample, zones of reduced electrical resistance were made visible as dark spots. For the µs-DBD-treated samples these distinct zones were clearly visible when the experiment was performed immediately after the plasma-treatment (within 5 min) or after 24 h (see Fig. 5). For untreated control samples or ns-DBD-treated SC no zones of decreased electrical resistance were detected.

Thus, both methods showed that permeabilization takes place during treatment with both µs-pulsed DBDs but was not detectable for ns-DBD-treatment of isolated human SC.

In the next step the permeation of larger substances was tested. Fluorescein, fluorophore-labeled dextran molecules or fluorescent latex particles ranging in diameter from < 1 nm to 2 µm acted as easily detectable model substances (see Table 1). Fluorescein and the two FITC-labeled dextrans (4 kDa and 40 kDa) were able to pass through µs-DBD treated SC. No diffusion through control or ns-DBD treated SC was detected (see Fig. 6). The 200 nm and 2 µm particles did not permeate through any SC samples (data not shown).

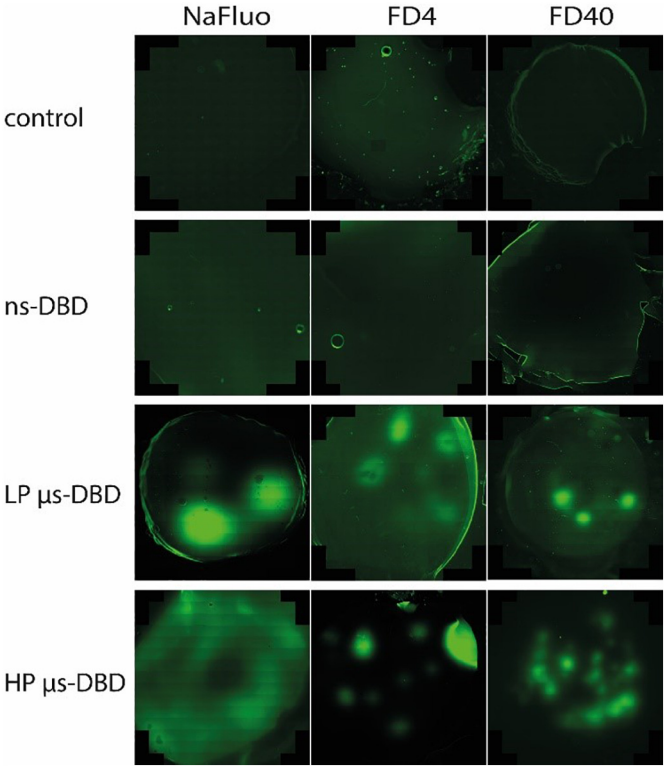

Fig. 6. Permeation of fluorescent test substances through DBD-treated or control SC. The total image size is 13.62 mm × 13.63 mm and each image is assembled from 186 tiles. For the LP µs-DBD the treatment regime differed. For this experiment the samples for the sodium fluorescein (NaFluo) and 40 kDa FITC-dextran (FD40) permeation had been treated 1 × 180 s, the samples for the 4 kDa FITC-dextran (FD4) permeation had been treated for 3× 90s.

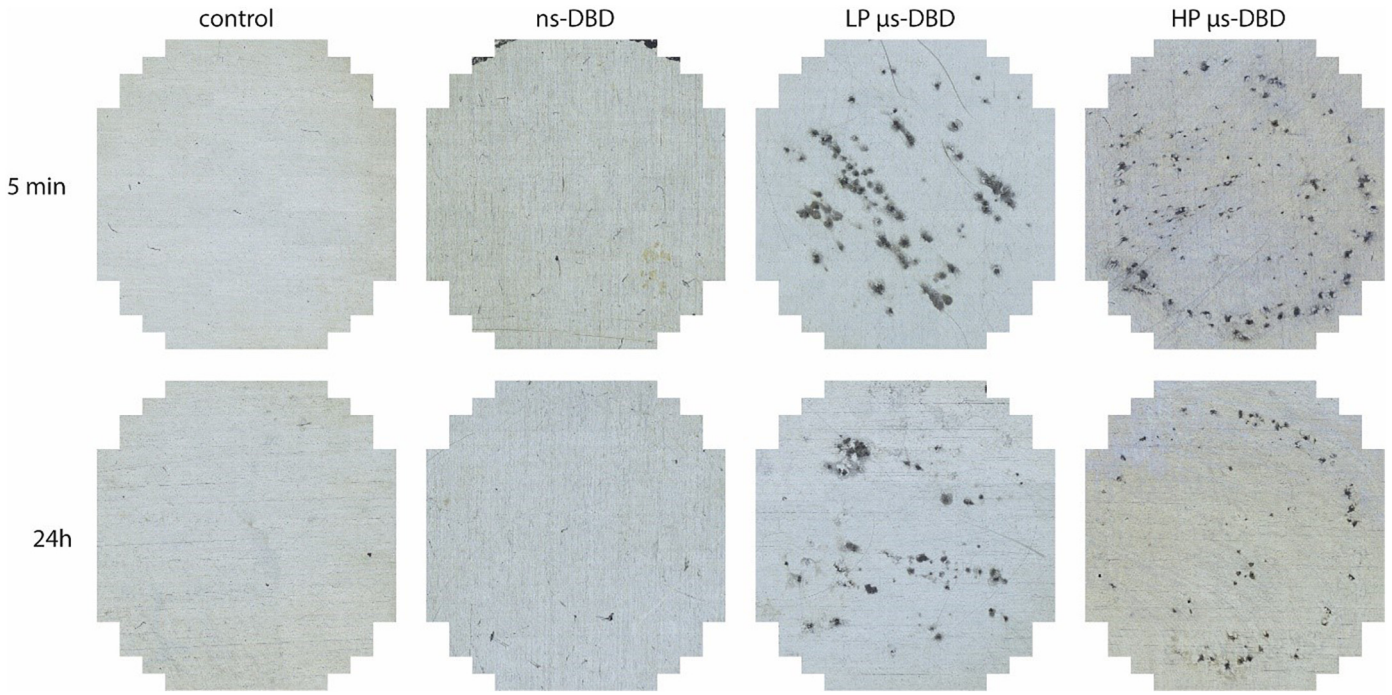

Fig. 5. Images of conductive regions formed in SC after DBD-treatment. Electrolytic images of a treated SC sample were produced immediately (5 min) and one day (24 h) after DBD-treatment. For each individual image the total dimensions are 10.5 × 10.9 mm and they are assembled from 208 tiles.

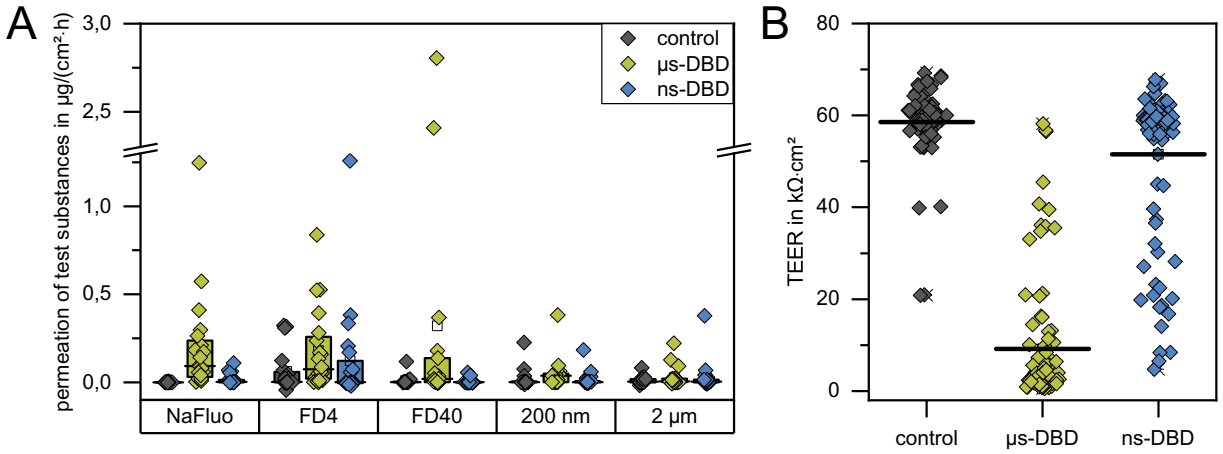

Fig. 7. Comparison of the permeabilization caused by a µs-pulsed and a ns-pulsed DBD of approximately the same power density. A) Permeation of test substances across control and DBD-treated human isolated stratum corneum (SC). In addition to the individual data (scatter plot, $n = 20$), box plots showing the median and the 25% and 75% quartile are depicted. B) Transepithelial electrical resistance (TEER) of control and DBD-treated SC ($n = 97–98$). Individual data as scatter plot are shown in addition to lines indicating the arithmetic mean. The pairwise differences between all groups are highly statistically significant; $p > > 0.001$.

3.3. Quantitative permeation of test substances

Quantitative permeation experiments were performed in Franz diffusion cells. As donor, the fluorescent molecules and particles were dissolved/suspended in a hydrogel – similar to a formulation that could be employed to deliver active pharmaceutical ingredients to the skin.

During the permeation experiments, the transepithelial electrical resistance (TEER) was recorded simultaneously, both as measure for sample quality [34], but also as a second measurement of permeabilization. When, in initial experiments, the TEER was measured in larger diffusion cells (inner diameter 15 mm) immediately before and after a 2×90 s LP µs-DBD treatment, the mean drop in resistance was 80 ± 73 kΩ·cm^2, which was significantly different ($p < < 0.001$) from control samples where the mean difference was -12 ± 31 kΩ·cm^2. In all further experiments smaller diffusion cells were used, which made DBD-treatment inside the diffusion cell impossible. Thus, TEER was recorded at the start of each experiment and after 24 h. Looking at the comparison of the two plasma sources with similar power density, the LP µs-DBD and the ns-DBD, concurrent with the permeation imaging experiments (Fig. 6), enhanced permeation of test substances up to 9 nm in diameter (FD40) was observed for the LP µs-DBD (Fig. 7). For the ns-DBD treated samples, the permeation of test substances was generally not meaningfully altered as compared to control samples. In post-hoc analysis the ns-DBD treatment always occurred in one homogeneous subset with the control. Nonetheless, a few ns-DBD treated samples were permeabilized, as seen by the 'comet tail' of the TEER signal down to lower resistance values (Fig. 7B) and in the permeation results in Fig. 7A. For the three smaller substances (NaFluo, FD4, FD40) the median permeation through LP µs-DBD treated SC was shown to be significantly different from ns-DBD treated SC as the two treatments were never part of the same homogeneous subset in the stepwise post-hoc analysis. For the 200 nm and the 2 µm particles the median permeations of all groups were analyzed not to differ significantly.

When the two µs-DBD sources of differing power density are compared, data show an increased permeabilization effect for the HP µs-DBD. The drop in TEER is more uniform and the permeation of test substances is facilitated even further (Fig. 8) as compared to the LP µs-DBD. The median permeation through HP µs-DBD treated SC was significantly different from both, the permeation through LP µs-DBD treated SC and control SC. The frequency of large particles (200 nm and 2 µm) passing through the HP µs-DBD treated SC is also slightly higher even though the median permeation of all groups was analyzed not to differ significantly for the particle permeation. Depending on the intended application of this technique, a penetration of large particles into the skin might be undesirable, as it could potentially increase the risk of infection.

In addition, preliminary permeation experiments performed with the hydrophobic Nile Red molecule in paraffin oil also show an improved permeation through µs-DBD treated skin. If compared to untreated SC, the median permeated amount after 24 h increased by a factor of 9.4 for LP µs-DBD treated SC and a factor of 11.9 for HP µs-DBD treated SC. A slightly enhanced permeation through ns-DBD treated SC was also observed (median permeated amount increased by a factor of 2.3).

From our experiments we can deduce that the electric characteristics of the voltage pulses used to create a discharge (µs-pulsed vs. ns-pulsed voltage) are more important than the resulting power density – which is practically the same for the ns-DBD and the LP µs-DBD – for permeabilization of human SC. Still, an increase in the power density did also increase the permeabilization efficiency for µs-pulsed DBD treatments.

3.4. Role of global heating and RONS-formation

Eventually, experiments were performed to further elucidate the mechanism of permeabilization by DBD treatment and address potential side-effects of a DBD treatment. Infrared photographs taken at the observed time of maximal heating of the samples at the end of a 90 s treatment show a maximal heating to 28.6 °C (Fig. 9). Since the phase transition temperatures of epidermal lipids has been reported to be much higher [35], one main transition occurs at 65 °C, global heating of the samples is not sufficient to cause permeabilization of the skin for all three DBDs. Heating of the surrounding air was determined to be negligibly small. For the HP µs-DBD the increase in temperature 1 cm from the discharge was 1.3 °C, 0.4 °C for the LP µs-DBD and no difference was detected for the ns-DBD.

Oxidation of skin lipids has recently been proposed as a mechanism for facilitation of drug delivery through ns-DBD-treated skin by Van der Paal et al. [16]. We determined the concentration of two relatively stable products of the chemical processes within DBDs, nitrate and peroxides, on the surface of treated SC (Fig. 10) and the ozone concentration in the gas phase (see Table 2) in order to compare the relative amount of reactive oxygen and nitrogen species (RONS) formed in the three DBDs.

The highest mean peroxide and nitrate concentrations are reached after ns-DBD treatment of SC. The values for the two µs-DBDs are lower. Since the 'oxidative potential' does not correlate with the observed

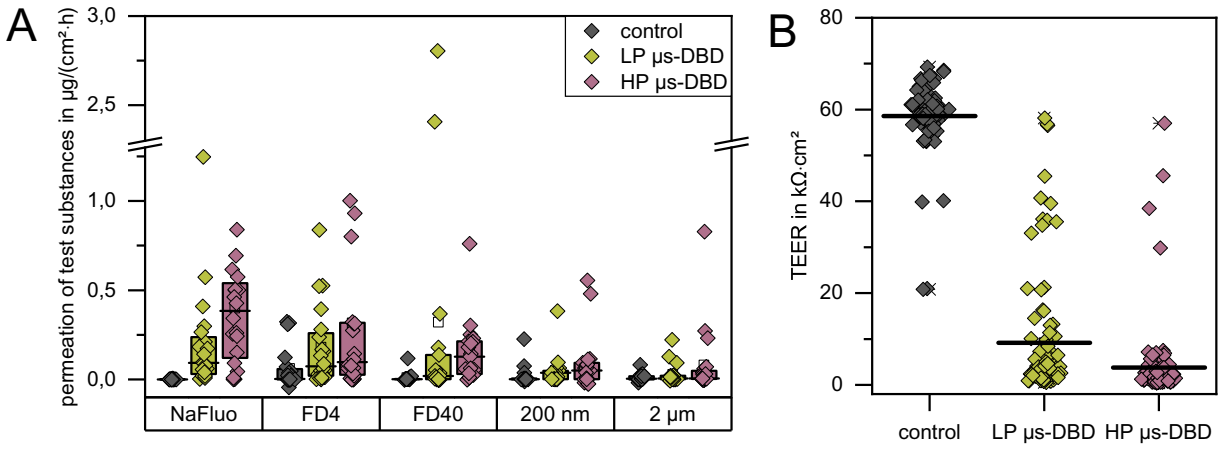

Fig. 8. Comparison of the permeabilization caused by two µs-pulsed DBDs differing in power density: The LP µs-DBD (low power µs-pulsed DBD); and the HP µs-DBD (high power µs-pulsed DBD). A) Permeation of test substances across control and DBD-treated human isolated stratum corneum (SC). In addition to the individual data (scatter plot, $n = 20$), box plots showing the median and the 25% and 75% quartile are depicted. B) Transepithelial electrical resistance (TEER) of control and DBD-treated SC ($n = 97–98$). Individual data as scatter plot are shown in addition to lines indicating the arithmetic mean. The pairwise differences between all groups are highly statistically significant; $p > > 0.001$.

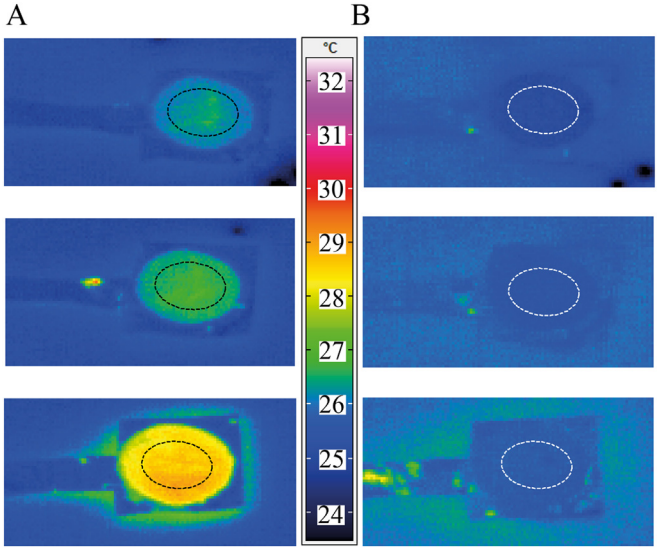

Fig. 9. Infrared images of SC treated with different DBDs. Dashed circles mark the area of the sample which has been exposed to the plasma. A) Circular samples of SC immediately (1 s) after a 90 s treatment with the ns-pulsed DBD (top), LP µs-pulsed DBD (center) and HP µs-pulsed DBD (bottom). With the background temperature at 25.2 °C, the maximum temperatures reached are 26.5 °C for ns-DBD treatment, 26.8 °C for the LP µs-DBD and 28.6 °C for the HP µs-DBD. B) 1 min after the end of the DBD treatment, as these images of the same samples shown in A illustrate, the SC temperature returns to room temperature quickly (top: ns-DBD, center: LP µs-DBD, bottom: HP µs-DBD).

permeabilization efficiency, we do not expect lipid oxidation to be the main permeabilization mechanism here. We would rather expect the filamentous nature of the µs-pulsed discharges (Fig. 1C), with their locally increased currents and temperatures (see rotational and vibrational temperatures in Table 2) to play the leading role in a mechanism based on 'Joule heating'. This has also been proposed to be the effect responsible for skin permeabilization through electroporation [36]. In order to further investigate the effect of lipid oxidation observed by Van der Paal et al., future studies would need to include a ns-pulsed DBD with higher amplitude or substantially longer treatment times.

To evaluate the potential effect of the peroxide concentrations reached after the DBD treatments, it is useful to compare them to a common treatment: A 100 µL drop of a 3% peroxide solution, which is commonly used for wound disinfection, on an area of 1 cm^2 will result in a peroxide concentration of 88 µmol·cm^{-2}. Compared to this, the values measured after DBD treatment are smaller by three orders of magnitude, and thus unlikely to damage the tissue significantly. For nitrate no acute toxic effects are to be expected upon contact with the skin, since only ingested nitrate/nitrite has been connected to the development of cancer in the digestive tract. Thus, we expect no direct toxic effects from peroxides or nitrate deposited during the plasma treatment. Ozone concentrations are at potentially toxic levels at 1 cm distance from the electrode. However, they decrease exponentially with increasing distance to the discharge. At a lateral distance of 10 cm the ozone concentrations were below the short term exposure level (STEL) of 0.3 ppm defined by the California Division of Occupational Safety and Health (Cal/OSHA) for all three plasma sources (data not shown) [28,37]. As long as the face is excluded as a treatment site, no additional safety measures should be necessary and no adverse effects are expected due to ozone toxicity for the treatment times used in our studies. The disinfecting properties of a cold atmospheric plasma treatment due to the creation of RONS may even be an additional desirable effect of given treatment modalities [20]. On the other hand, depending on the type of drug subsequently used for transdermal delivery, a relatively low concentration of oxidizing species could be beneficial in order to avoid modifications of the drug molecules.

3.5. Suitability of the tested plasma sources for drug delivery

Combining the results from peroxide, nitrate and ozone measurements with the permeabilization observed above, the LP µs-DBD would be the most favorable option for a safe and pain-free method to enhance drug delivery. The HP µs-DBD is more efficient, but produces more nitrate and ozone in addition to being more painful (personal observation). The ns-DBD, on the other hand, would be suitable for treatment options that harness the therapeutic effects of the chemical species while keeping the skin barrier intact. Or, since a ns-DBD treatment was not observed to elicit any pain during treatment and a small permeabilizing effect was observed, longer treatment durations might enhance the limited effect of permeabilization observed here.

If implemented as a drug delivery tool, this method would be useful to enhance the permeation of hydrophilic drug molecules up to 9 nm in size and small lipophilic substances. This could include sensitive biological molecules such as proteins or nucleic acids. Whether the permeation of lipophilic compounds in the ns-range is likewise enhanced, will be the subject of further studies.

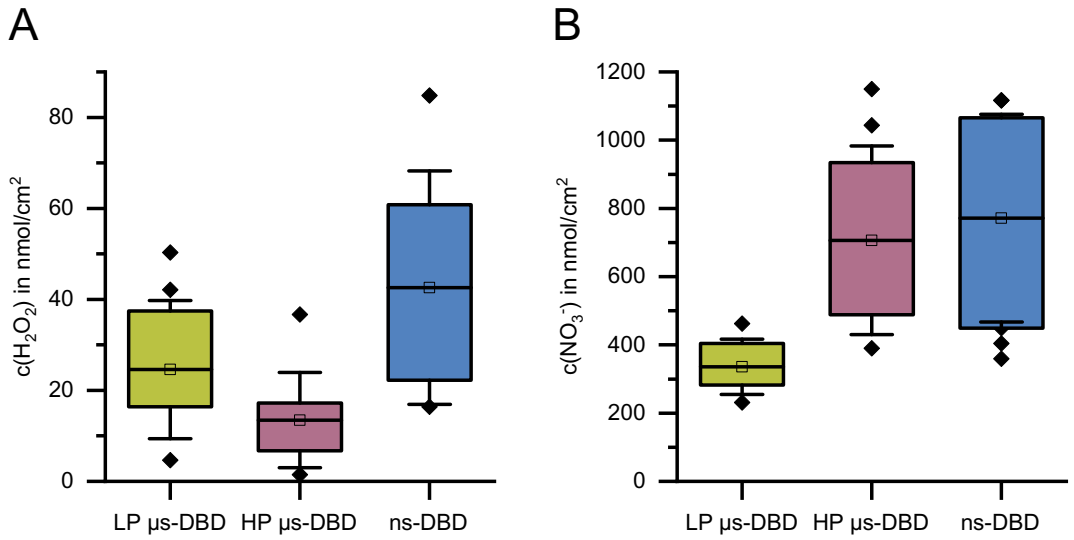

Fig. 10. Chemical species produced on the DBD-treated SC surface. A) Peroxide concentration after 90 s of DBD-treatment. Measured inside a 200 µL drop applied immediately after the treatment and given as concentration of H_2O_2 per cm^2 of treated SC. $n = 9$. B) Nitrate concentration per cm^2 of treated SC measured in the same drop after the peroxide measurement. n = 9. For A and B) Box plots show the mean, the 25% and 75% percentiles and the standard deviation (whiskers). Outliers are shown as black diamonds. *) $p \leq .05$; **) $p \leq .01$.

In general, the permeabilization of human skin by µs-DBD was a robust effect. Nevertheless, we observed large differences in the degree of pore formation between different samples. Thus, for medical applications, it would be beneficial to monitor the permeabilization during the treatment and stop once a sufficient permeabilization has been achieved – the treatment regime used here (90 s increments with a rest period in between) is suitable for the combination with a noninvasive measurement.

So far we have not been successful in implementing the measurement of TEER during treatment as a substantial liquid layer is needed for reliable measurements, and this hampers the plasma ignition. However, given a suitable setup, it should be possible to apply a measurement of the transepidermal water loss (TEWL) during the treatment pause. Since infrared imaging showed the return of the temperature of SC samples to room temperature in < 1 min after the end of a DBD treatment, no perturbation of a TEWL measurement is to be expected.

4. Conclusion

Use of direct cold atmospheric plasma on human isolated stratum corneum shows high potential for application in different treatment settings. Depending on pulse characteristics (voltage rise time, maximum voltage amplitude) the plasma can be tuned to be suitable as a safe and pain-free tool for skin permeabilization, but also, with different parameters, as a therapeutic device or treatment modality to deliver therapeutically effective plasma components to a patients skin without damaging it, e.g. in skin diseases like psoriasis or to treat pruritus. Due to the slightly unstable nature of DBDs in changing environmental settings it would be beneficial for future developments to have a method for the immediate determination of the outcome of a treatment. This would enable the practitioner to tune, e.g., the treatment duration to each patient's needs. As this method needs to be fast and non-invasive, one example would be the commonly determined transepidermal water loss (TEWL) as a measure for the dermal barrier function.

Acknowledgements

The authors would like to thank Dr. Jennifer Ernst and Dr. Gunther Felmerer at the Department of Trauma-, Orthopedic- and Plastic Surgery of the University Medical Center Göttingen for their continued help with the provision of donated skin.

Funding

This work was supported by a Georg-Christoph-Lichtenberg grant to Monika Gelker through the PhD Program *Processing of poorly soluble drugs at small scale*, funded by Lower Saxony's Ministry of Science and Culture (MWK) and the German Federal Ministry of Education and Research (FKZ: 03FH015IX5 and FKZ: 13FH6E01IA).

Funding sources had no influences in study design; in the collection, analysis and interpretation of data; in the writing of the report; and in the decision to submit the article for publication.

Conflict of interest

The authors declare no conflict of interest.

References

[1] T. Waghule, G. Singhvi, S.K. Dubey, M.M. Pandey, G. Gupta, M. Singh, K. Dua, Microneedles: a smart approach and increasing potential for transdermal drug delivery system, Biomed. Pharmacother. 109 (2019) 1249–1258, https://doi.org/10.1016/j.biopha.2018.10.078.

[2] K. Ita, Perspectives on transdermal electroporation, Pharmaceutics 8 (2016) 9, https://doi.org/10.3390/pharmaceutics8010009.

[3] B.C.-Q. Seah, B.M. Teo, Recent advances in ultrasound-based transdermal drug delivery, Int. J. Nanomedicine 13 (2018) 7749–7763, https://doi.org/10.2147/IJN.S174759.

[4] M. Yusupov, J. Van der Paal, E.C. Neyts, A. Bogaerts, Synergistic effect of electric field and lipid oxidation on the permeability of cell membranes, Biochim. Biophys. Acta Gen. Subj. 1861 (2017) 839–847, https://doi.org/10.1016/j.bbagen.2017.01.030.

[5] M. Gelker, C.C. Müller-Goymann, W. Viöl, Permeabilization of human stratum corneum and full-thickness skin samples by a direct dielectric barrier discharge, Clin. Plasma Med. 9 (2018) 34–40, https://doi.org/10.1016/j.cpme.2018.02.001.

[6] G. Isbary, T. Shimizu, Y.-F. Li, W. Stolz, H.M. Thomas, G.E. Morfill, J.L. Zimmermann, Cold atmospheric plasma devices for medical issues, Expert Rev. Med. Dev. 10 (2014) 367–377, https://doi.org/10.1586/ERD.13.4.

[7] T. Borchardt, J. Ernst, A. Helmke, M. Tanyeli, A.F. Schilling, G. Felmerer, W. Viöl, Effect of direct cold atmospheric plasma (diCAP) on microcirculation of intact skin in a controlled mechanical environment, Microcirculation 24 (2017), https://doi.org/10.1111/micc.12399.

[8] T. Kisch, A. Helmke, S. Schleusser, J. Song, E. Liodaki, F.H. Stang, P. Mailaender, R. Kraemer, Improvement of cutaneous microcirculation by cold atmospheric plasma (CAP): results of a controlled, prospective cohort study, Microvasc. Res. 104 (2016) 55–62, https://doi.org/10.1016/j.mvr.2015.12.002.

[9] A. Helmke, D. Hoffmeister, N. Mertens, S. Emmert, J. Schuette, W. Vioel, The acidification of lipid film surfaces by non-thermal DBD at atmospheric pressure in air, New J. Phys. 11 (2009) 115025, , https://doi.org/10.1088/1367-2630/11/11/115025.

[10] G. Isbary, T. Shimizu, J.L. Zimmermann, J. Heinlin, S. Al-Zaabi, M. Rechfeld, G.E. Morfill, S. Karrer, W. Stolz, Randomized placebo-controlled clinical trial showed cold atmospheric argon plasma relieved acute pain and accelerated healing in herpes zoster, Clin. Plasma Med. 2 (2014) 50–55, https://doi.org/10.1016/j.cpme.2014.07.001.
[11] J. Kristof, T. Aoshima, M. Blajan, K. Shimizu, Surface modification of stratum corneum for drug delivery and skin care by microplasma discharge treatment, Plasma Sci. Technol. (2019), https://doi.org/10.1088/2058-6272/aafde6.
[12] O. Lademann, H. Richter, M.C. Meinke, A. Patzelt, A. Kramer, P. Hinz, K.-D. Weltmann, B. Hartmann, S. Koch, Drug delivery through the skin barrier enhanced by treatment with tissue-tolerable plasma, Exp. Dermatol. 20 (2011) 488–490, https://doi.org/10.1111/j.1600-0625.2010.01245.x.
[13] J.-H. Choi, S.-H. Nam, Y.-S. Song, H.-W. Lee, H.-J. Lee, K. Song, J.-W. Hong, G.-C. Kim, Treatment with low-temperature atmospheric pressure plasma enhances cutaneous delivery of epidermal growth factor by regulating E-cadherin-mediated cell junctions, Arch. Dermatol. Res. 306 (2014) 635–643, https://doi.org/10.1007/s00403-014-1463-9.
[14] K. Shimizu, K. Hayashida, M. Blajan, Novel method to improve transdermal drug delivery by atmospheric microplasma irradiation, Biointerphases 10 (2015) 29517, , https://doi.org/10.1116/1.4919708.
[15] S. Kalghatgi, C. Tsai, R. Gray, D.D. Pappas, Transdermal Drug Delivery Using Cold Plasmas, 22nd International Symposium on Plasma Chemistry, (2015) (Antwerp, Belgium).
[16] Jonas Van der Paal, G. Fridman, A. Fridman, E.C. Neyts, A. Bogaerts, In search of the plasmaporation mechanism during plasma treatment of skin, 4th International Workshop on Plasma for Cancer Treatment (IWPCT-2017), Paris, 2017.
[17] A.M. Kligman, E. Christophers, Preparation of isolated sheets of human stratum corneum, Arch. Dermatol. 88 (1963) 702–705.
[18] A. Helmke, D. Wandke, M. Mahmoodzada, K.-D. Weltmann, W. Viöl, Impact of electrode design, supply voltage and Interelectrode distance on safety aspects and characteristics of a medical DBD plasma source, Contrib. Plasma Phys. 53 (2013) 623–638, https://doi.org/10.1002/ctpp.201200133.
[19] Z. Machala, M. Janda, K. Hensel, I. Jedlovský, L. Leštinská, V. Foltin, V. Martišovitš, M. Morvová, Emission spectroscopy of atmospheric pressure plasmas for bio-medical and environmental applications, J. Mol. Spectrosc. 243 (2007) 194–201, https://doi.org/10.1016/j.jms.2007.03.001.
[20] D.B. Graves, The emerging role of reactive oxygen and nitrogen species in redox biology and some implications for plasma applications to medicine and biology, J. Phys. D. Appl. Phys. 45 (2012) 263001, , https://doi.org/10.1088/0022-3727/45/26/263001.
[21] J. Hirschberg, T. Omairi, N. Mertens, A. Helmke, S. Emmert, W. Viöl, Influence of excitation pulse duration of dielectric barrier discharges on biomedical applications, J. Phys. D. Appl. Phys. 46 (2013) 165201, , https://doi.org/10.1088/0022-3727/46/16/165201.
[22] F. Peters, B. Hünnekens, S. Wieneke, H. Militz, G. Ohms, W. Viöl, Comparison of three dielectric barrier discharges regarding their physical characteristics and influence on the adhesion properties on maple, high density fiberboards and wood plastic composite, J. Phys. D. Appl. Phys. 50 (2017) 475206, , https://doi.org/10.1088/1361-6463/aa8fad.
[23] F. Peters, B. Hünnekens, S. Wieneke, H. Militz, G. Ohms, W. Viöl, Corrigendum: comparison of three dielectric barrier discharges regarding their physical characteristics and influence on the adhesion properties of maple, high density fiberboard and wood plastic composite (2017 J. Phys. D: Appl. Phys 50 475206), J. Phys. D. Appl. Phys. 51 (2018) 159501, , https://doi.org/10.1088/1361-6463/aab378.
[24] P. Paris, M. Aints, F. Valk, T. Plank, A. Haljaste, K.V. Kozlov, H.-E. Wagner, Intensity ratio of spectral bands of nitrogen as a measure of electric field strength in plasmas, J. Phys. D. Appl. Phys. 38 (2005) 3894–3899, https://doi.org/10.1088/0022-3727/38/21/010.
[25] S. Pancheshnyi, Comments on ‘intensity ratio of spectral bands of nitrogen as a measure of electric field strength in plasmas’, J. Phys. D. Appl. Phys. 39 (2006) 1708–1710, https://doi.org/10.1088/0022-3727/39/8/N01.
[26] P. Paris, M. Aints, F. Valk, T. Plank, A. Haljaste, K.V. Kozlov, H.-E. Wagner, Reply to comments on ‘intensity ratio of spectral bands of nitrogen as a measure of electric field strength in plasmas’, J. Phys. D. Appl. Phys. 39 (2006) 2636–2639, https://doi.org/10.1088/0022-3727/39/12/N01.
[27] R. Tiede, J. Hirschberg, W. Viöl, S. Emmert, A us-pulsed dielectric barrier discharge source: physical characterization and biological effects on human skin fibroblasts, Plasma Process. Polym. 13 (2016), https://doi.org/10.1002/ppap.201500190.
[28] L. ten Bosch, B. Habedank, D. Siebert, J. Mrotzek, W. Viöl, Cold atmospheric pressure plasma comb-aphysical approach for pediculosis treatment, Int. J. Environ. Res. Public Health 16 (2018), https://doi.org/10.3390/ijerph16010019.
[29] U.F. Pliquett, T.E. Zewert, T. Chen, R. Langer, J.C. Weaver, Imaging of fluorescent molecule and small ion transport through human stratum corneum during high voltage pulsing: localized transport regions are involved, Biophys. Chem. 58 (1996) 185–204.
[30] J. Fokuhl, C.C. Müller-Goymann, Untersuchung der Unversehrtheit von humanem exzidiertem Stratum corneum mittels TEER-Messungen, DPhG-Jahrestagung, Erlangen, (October 10th–13th, 2007).
[31] T.J. Franz, Percutaneous absorption. On the relevance of in vitro data, J. Investig. Dermatol. 64 (1975) 190–195, https://doi.org/10.1111/1523-1747.ep12533356.
[32] A. Täuber, C.C. Müller-Goymann, In vitro permeation and penetration of ciclopirox olamine from poloxamer 407-based formulations—comparison of isolated human stratum corneum, bovine hoof plates and keratin films, Int. J. Pharm. 489 (2015) 73–82, https://doi.org/10.1016/j.ijpharm.2015.04.043.
[33] S. Lusiana, C.C. Müller-Goymann Reichl, Keratin film made of human hair as a nail plate model for studying drug permeation, Eur. J. Pharm. Biopharm. 78 (2011) 432–440, https://doi.org/10.1016/j.ejpb.2011.01.022.
[34] K. Guth, M. Schäfer-Korting, E. Fabian, R. Landsiedel, B. van Ravenzwaay, Suitability of skin integrity tests for dermal absorption studies in vitro, Toxicol. in Vitro 29 (2015) 113–123, https://doi.org/10.1016/j.tiv.2014.09.007.
[35] I. Plasencia, L. Norlén, L.A. Bagatolli, Direct visualization of lipid domains in human skin stratum corneum's lipid membranes: effect of pH and temperature, Biophys. J. 93 (2007) 3142–3155, https://doi.org/10.1529/biophysj.106.096164.
[36] U. Pliquett, S. Gallo, S.W. Hui, C. Gusbeth, E. Neumann, Local and transient structural changes in stratum corneum at high electric fields: contribution of Joule heating, Bioelectrochemistry 67 (2005) 37–46, https://doi.org/10.1016/j.bioelechem.2004.12.003.
[37] California Division of Occupational Safety and Health, Table AC-1, Permissible Exposure Limits (PELs), https://www.osha.gov/chemicaldata/chemResult.html?RecNo=9 , Accessed date: 6 March 2019.